ACS Catalysis

pubs.acs.org/acscatalysis

Research Article

Unraveling Intrinsic Electronic Factors in Thermocatalytic (Hemi-) Hydrogenation of Ethylene and Acetylene with Electric Polarization

Qikai Shen,[§] Hanwen Yang,[§] Kaiyue Zhao, Leyu Liu, Qiwen Sun, Xiaoxia Chang, Hai Xiao,* and Bingjun Xu*

Cite This: *ACS Catal.* 2023, 13, 14570−14579

Read Online

ACCESS | Metrics & More | Article Recommendations | Supporting Information

ABSTRACT: Favorable electronic interactions between active sites and substrates or transition states are essential to promoting a catalytic reaction. However, tuning the electronic state is often coupled with compositional or structural changes of active sites, leading to uncertainties in the catalyst design. Herein, we isolate the impact of the Fermi level of Pt, Pd, and Rh nanoparticles on thermocatalytic (hemi)hydrogenation of ethylene and acetylene with electric polarization. Through a combination of kinetic, spectroscopic, isotopic labeling, and computational investigations, we show that the electric polarization by applying a potential bias tunes the rate and product distribution of ethylene hydrogenation by altering the coverages of key intermediates, e.g., hydrogen, acetonitrile, and ethylene. The proposed mechanistic framework rationalizes the simultaneous increase in the rate and selectivity of acetylene hydrogenation on Pt as the Fermi level is increased by applying a negative potential bias. This work highlights the promise of leveraging electric polarization as a strategy to advance the mechanistic understanding and optimize performance in heterogeneous catalysis.

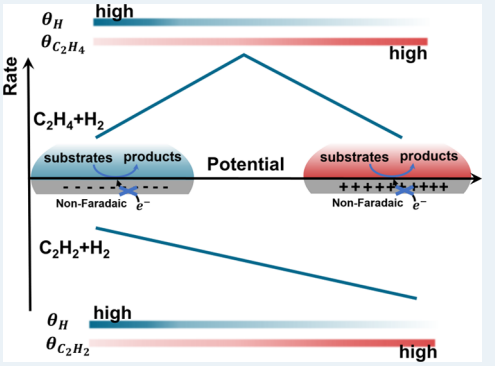

KEYWORDS: *hydrogenation of ethylene and acetylene, electric polarization, Fermi level, thermocatalysis, intrinsic electronic factors*

INTRODUCTION

Elucidating structure−activity relations has long been considered as the central task in the catalysis research,[1−5] based on the well-accepted assumption that the performance in thermocatalytic reactions depends exclusively on the structure of catalysts at a given set of reaction conditions. Activation of substrates and stabilization of transition states require favorable electronic interactions with the active sites, which are predicated on both configurational and energetic matches between the substrate and the active site. For metal catalysis, the energetic match is primarily controlled by the Fermi level of the metal sites, which can be tuned via multiple strategies, such as modifying the support[6−10] and introducing promoters.[11−14] However, these Fermi level tuning strategies typically alter either the composition or the structure of catalysts, if not both, leading to ambiguities in the mechanistic interpretations. Supports could shift the Fermi level of supported metal nanoparticles by either donating or abstracting electrons.[15,16] When supported on CeO_2, Pt nanoparticles were reported to lose up to 0.11 electron to the support per Pt atom[17] and thus became positively charged with a lower Fermi level. Meanwhile, the interfacial sites between the metal nanoparticles and the support are highly support dependent and in many cases are the most catalytically active,[18−20] e.g., the interfacial Pt−Nb alloy sites on Pt/Nb_2CT_x MXene have been reported to enhance the kinetics of the water−gas shift reaction.[21] Deconvolution of the electronic effect on metal catalysis from the chemical effect specific to the support material is often a topic of discussion in the literature.[8,12,22−26] In this regard, non-Faradaic electrochemical modification of catalytic activity (NEMCA), initially proposed by Huggins, Mason, and co-workers[27] and later developed by Vayenas and co-workers,[28,29] offers a conceptually straightforward method to isolate the effect of the Fermi level of metals on catalytic performance.

With NEMCA, thermocatalytic reactions occur at an electrified interface while Faradaic processes do not contribute appreciably to the formation of products.[28−33] The Fermi level of catalysts is directly controlled by an external power source without changing the catalyst structure, affording the possibility of establishing a direct correlation between the electronic state of the catalyst and the catalytic performance. Early NEMCA studies were largely conducted on high-temperature electrochemical interfaces with solid inorganic electrolytes.[27,30,31,34,35] Migrations of ionic species to catalytic interfaces complicate the interpretation of the effect of the applied potential on the activity.[28,36,37] Recent studies showed that electric polarization could have a significant impact on the reaction rates at close to

Received: September 8, 2023
Revised: October 9, 2023
Accepted: October 12, 2023
Published: October 30, 2023

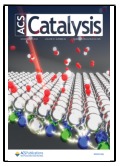

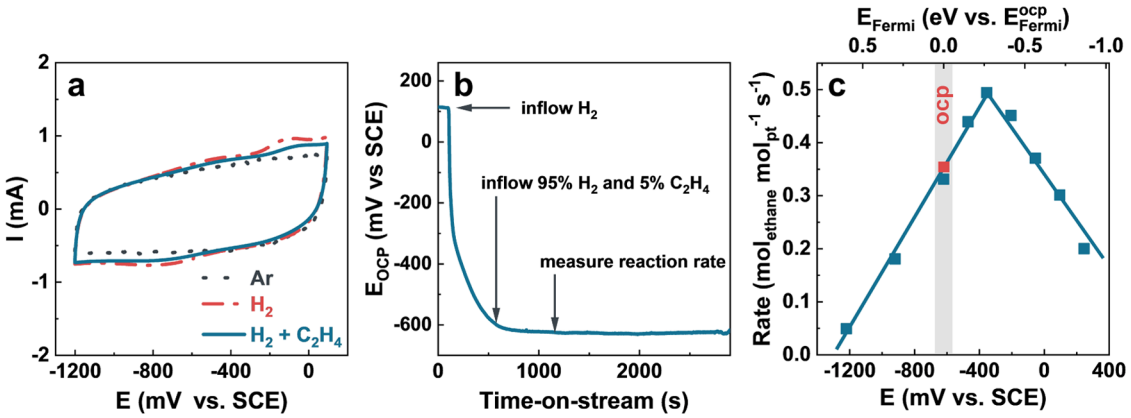

Figure 1. (a) Cyclic voltammograms of Pt/C in acetonitrile with 0.1 M $[P_4N]PF_6$ under different atmospheres. (b) Evolution of E_{ocp} under different atmospheres (indicated in the figure). (c) Dependence of ethylene hydrogenation rate on the applied potential on Pt/C.

ambient conditions in aqueous electrolytes without affecting the structure of the catalysts,[38−49] highlighting the feasibility of leveraging electric polarization to isolate the impact of the Fermi level on the rate on metal-catalyzed reactions. However, the mechanistic understanding of the pathways through which electric polarization of the catalyst impacts the performance, especially the product distribution, of thermocatalytic reactions remains incomplete.

In this work, we demonstrate that both the rate and the product distribution of ethylene and acetylene hydrogenation can be tuned by the externally applied potential on supported Pt, Pd, and Rh catalysts. Through a combination of kinetic, spectroscopic, isotopic labeling, and computational investigations, we show that shifts in the Fermi level impact the reaction orders of substrates and the surface coverages of adsorbed intermediates. Kinetic modeling based on a modified Horiuti−Polanyi mechanism is able to predict the volcano-shaped dependence of ethylene hydrogenation rate on the applied potential. Rate of acetylene hydrogenation, as well as the selectivity for ethylene, is enhanced at more negative potentials (higher Fermi levels), which could be rationalized by the weakened adsorption energy of acetylene and ethylene on Pt.

RESULTS AND DISCUSSION

Impact of Electric Polarization on Pt-, Pd-, and Rh-Catalyzed Ethylene Hydrogenation. To isolate the non-Faradaic effect of the electric polarization on precious metal-catalyzed ethylene hydrogenation, reaction conditions were chosen to minimize the potential impact of Faradaic processes on the measured rates. Ethylene hydrogenation reaction was conducted on Pt/C in acetonitrile with 0.1 M $[P_4N]PF_6$ as an electrolyte in a H-type cell (Figure S1). Transmission electron microscopy images show that the average size of Pt nanoparticles in Pt/C is ∼3 nm (Figure S2a), which agrees with the broad X-ray powder diffraction (XRD) peaks (Figure S2b). Pt/C treated with H_2 at room temperature was characterized by X-ray photoemission spectroscopy without air exposure (quasi in situ XPS), which indicated that Pt was mostly in the metallic form (Figure S2c). Acetonitrile,—an aprotic solvent, is employed in the reaction because (1) it suppresses electrochemical hydrogenation of ethylene due to the lack of protons and (2) it affords a wide accessible potential window within which no appreciable electrochemical reactions occur, e.g., hydrogen and oxygen evolution reactions. The cyclic voltammogram (CV) of Pt in Ar does not show any discernible feature (Figure 1a), suggesting that the concentration of the residual water in acetonitrile is unlikely to provide sufficient protons to sustain appreciable electrochemical ethylene hydrogenation. This was confirmed by the lack of ethane formation when pure ethylene was used as the feed at −55 and 1200 mV (all potentials in this work are referenced to the saturated calomel electrode, or SCE, unless noted otherwise). The CV collected in H_2 (1 atm) shows two broad and weak bands at −150 and −500 mV in the anodic scan (Figure 1a), which are likely due to the oxidation of H_2.[50,51] The broad band located at −800 mV in the cathodic scan could be attributed to the reduction of protons produced in the anodic scan.[50−52] Both the anodic and cathodic features are suppressed in the CV collected in the H_2/ethylene atmosphere (95:5 vol %), which could be caused by the preferential adsorption of ethylene on Pt.[53−55] The weak CV features suggest that Faradaic processes in the current system are unlikely to affect the ethylene hydrogenation reaction.

Open-circuit potential (E_{ocp}) of Pt/C was monitored when reactants were introduced to the system (Figure 1b). E_{ocp} was measured to be ∼115 mV in air, which dropped precipitously when the atmosphere was switched to H_2. This could be attributed to the shifting of the redox pair pinning the potential of Pt/C, i.e., from O_2/H_2O (in air) to H_2/H^+ (in H_2),[56] where both H_2O and H^+ are present in the trace amount of residual water in acetonitrile. E_{ocp} stabilized after 10 min to ∼ −620 mV in the H_2 atmosphere. E_{ocp} remained unchanged when the atmosphere was switched from H_2 to the reactant mixture, i.e., H_2/ethylene (95:5 vol %). This entails that the presence of ethylene (5 vol %) does not impact the redox pair that pins the electrode potential.

Applied potential on Pt/C has a substantial and non-monotonic impact on the ethylene hydrogenation rate. A more negative potential corresponds to a higher Fermi level (top axis in Figure 1c, all Fermi level (E_{Fermi}) in this work is referenced to that at E_{ocp} (referred to as E^{ocp}_{Fermi}) unless noted otherwise). The ethylene hydrogenation rate increases almost linearly as the potential rises from −1220 to −355 mV, before declining with a further increase in the potential. A similar observation was made in the aqueous electrolyte, albeit in a narrower potential window.[41] The ethane production rate increases linearly by 0.52 $[mol_{ethane}\cdot mol_{Pt}\cdot s^{-1}]/V$ at more negative potentials before peaking at −355 mV and then decreases by 0.49 $[mol_{ethane}\cdot mol_{Pt}\cdot s^{-1}]/V$ at more positive potentials. As expected, the ethane production rate at −620 mV is consistent with that measured without an applied potential (E_{ocp}, shaded in Figure 1c). In the

https://doi.org/10.1021/acscatal.3c04258
ACS Catal. 2023, 13, 14570−14579

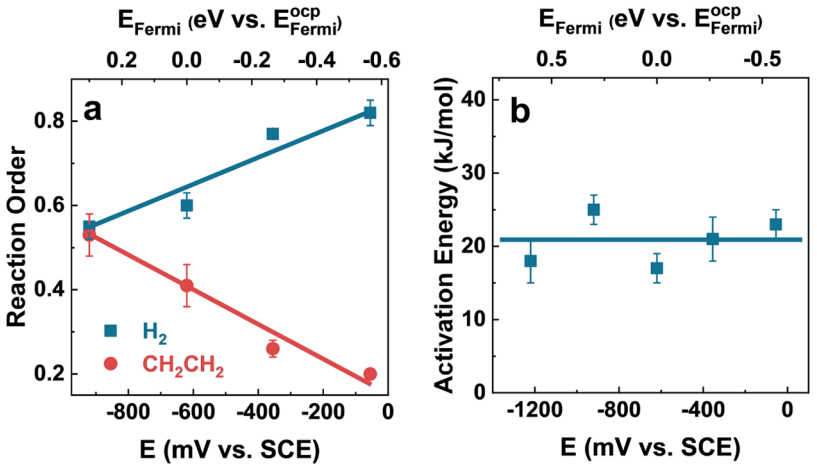

Figure 2. (a) Measured reaction orders of ethylene and hydrogen in ethylene hydrogenation at different applied potentials on Pt/C. (b) Activation energies of ethylene hydrogenation at different applied potentials on Pt/C.

potential range of −920 to −55 mV, the measured currents are at least 2 orders of magnitude smaller than values calculated assuming that all of the ethane is produced via a electrochemical reduction of ethylene (Figure S3a), i.e., the calculated Faradaic efficiency could reach up to 160 000% (Figure S3c), suggesting a negligible effect of the Faradaic process on the measured ethane production rates. Anodic current becomes significant at potentials above 245 mV (Figure S3b), likely corresponding to the electrochemical oxidation of hydrogen, which is consistent with the CV feature (Figure S4). Thus, only ethylene hydrogenation rates determined between −1220 and 95 mV were used in the mechanistic analysis below. Ethylene hydrogenation rates were measured in the kinetic regime, which was confirmed by the linear correlation between the absolute hydrogenation rates and the catalyst loading at −620 and 355 mV (Figure S5). Importantly, the ethane production rate at −355 mV is roughly 1 order of magnitude higher than that at −1220 mV, demonstrating the substantial impact of the electric polarization of the catalyst on the reaction rate.

Similar volcano-shaped dependence of the ethylene hydrogenation rate on the applied potential was also observed on Pd/C and Rh/C (Figure S6). The average diameter of both Pd and Rh nanoparticles is 3−5 nm (Figure S7), which is consistent with the line width in the corresponding XRD patterns (Figure S8). Quasi in situ XPS shows that while Pd exists mostly in the metallic form, ∼60% of Rh is present in the oxidized form with an average oxidation state of +3 (Figure S9). This is expected due to the greater oxophilicity of Rh compared to Pt and Pd.[57,58] E_{ocp} on Pd/C and Rh/C were measured to be −355 and −470 mV, respectively, both of which were different from that of Pt/C (Figure S10). The electrochemical equilibrium that determines E_{ocp} on metals could involve surface intermediates, e.g., H_{ad}/H^+, which is likely the cause of the metal dependence of E_{ocp}. The trend of ethane production rate with respect to the applied potential for Pd/C is similar to that of Pt/C, with the optimal ethylene hydrogenation activity at −355 mV. The ethane production rate on Pd/C increases by 0.59 [mol_{ethane}·mol_{Pd}·s^{-1}]/V at potentials below −355 mV and decreases by 0.34 [mol_{ethane}·mol_{Pd}·s^{-1}]/V at more positive potentials. The peak ethane production rate on Rh/C occurs at a significantly more negative potential (−1050 mV) than those on Pd/C and Pt/C. The ethylene hydrogenation rate is less sensitive to potential on Rh/C. The ethane production rate increases by 0.030 [mol_{ethane}·mol_{Rh}·s^{-1}]/V below the optimal potential on Rh/C, which is a factor of 17 lower than that on Pt/C. The observation of the volcano-shaped dependence of the ethane production rate on the applied potential suggests the universality of the impact of the electric polarization and the Fermi level of the metal catalyst on surface-mediated reactions.

Potential Dependence of Ethylene Hydrogenation Kinetics on Pt/C. Electric polarization and the associated change in the Fermi level have a significant effect on the reaction order of reactants but not the apparent activation energy (E_{app}). Reaction orders of ethylene and H_2 were determined to be both ∼0.55 at −920 mV on Pt/C (Figures 2a and S12). As the potential increases to −55 mV, the reaction order of ethylene decreases to ∼0.2, while that of H_2 increases to ∼0.8. Reaction orders of ethylene and H_2 on Pt/C at room temperature in a fixed bed reactor in the absence of acetonitrile were determined to be −0.5 and 0.8, respectively (Figure S13a), which were consistent with the literature.[59,60] The negative reaction order of ethylene indicates that the high coverage of ethylene limits the density of sites available for the dissociative adsorption of H_2 to form H_{ad} at the solid−gas interface without applied potential and acetonitrile.[59,61,62] Reaction orders of ethylene and H_2 on Pt/C determined in the fixed bed reactor (without any applied potential) with a saturated vapor pressure of acetonitrile at room temperature (20.3 kPa) in the feed were 0.4 and 0.7, respectively (Figure S13a). The positive reaction order of ethylene in the presence of acetonitrile suggests that the adsorption of acetonitrile significantly reduces the ethylene coverage. The ethane production rate with acetonitrile vapor is lower than that in the acetonitrile-free feed by a factor of ∼10 (Figure S13b), which is consistent with reduced coverages of ethylene and H_{ad} on the Pt surface due to the competitive adsorption of acetonitrile. Reaction orders of ethylene and H_2 determined with acetonitrile vapor in the feed on Pt/C (0.5 wt %) are similar to those determined when the catalyst (commercial Pt/C 5 wt %) is immersed in liquid acetonitrile solvent with electrolyte at −620 mV (E_{ocp}, Figure S13a). Coverages of ethylene and H_{ad} on Pt in the presence of acetonitrile vapor are likely comparable to those in liquid acetonitrile solvent. This is reasonable since a thin layer of acetonitrile likely adsorbs on the catalyst surface at its saturated vapor pressure, so that the two systems becomes comparable on the molecular level, i.e., the catalyst surface mostly covered by a liquid(-like) layer of acetonitrile. This claim

https://doi.org/10.1021/acscatal.3c04258
ACS Catal. 2023, 13, 14570−14579

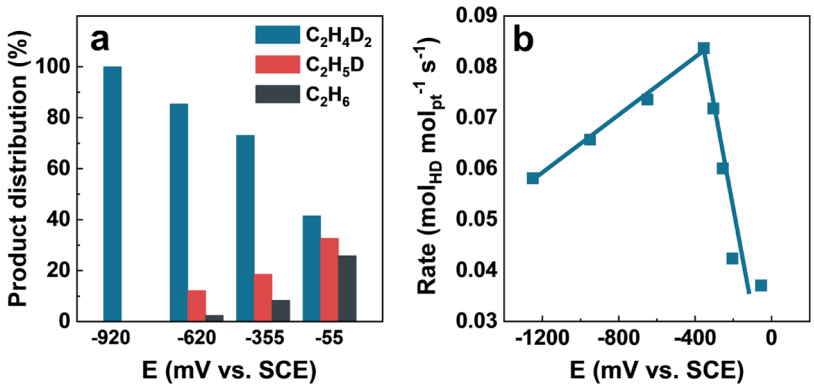

Figure 3. (a) Isotopic composition of produced ethane in the hydrogenation of ethylene with D_2 at different applied potentials on Pt/C. (b) H−D exchange rates in equimolar amounts of H_2 and D_2 at different applied potentials on Pt/C.

is supported by the comparable ethane production rates in the presence of saturated acetonitrile vapor and liquid acetonitrile (Figure S13b). Assuming ethylene hydrogenation occurs via a Langmuir−Hinshelwood-type mechanism involving surface-adsorbed ethylene and H,[63−65] reaction orders of ethylene and H_2 could be employed as qualitative measures of surface coverages of ethylene and H_{ad}, i.e., a lower reaction order of ethylene corresponds to a higher surface ethylene coverage, while a lower reaction order of H_2 indicates a lower coverage of H_{ad}. This hypothesis will be analyzed in more detail later in this work. E_{app} of ethylene hydrogenation on Pt/C were obtained by determining the ethane production rates in the range of 0−30 °C, which were in the range of 17−23 kJ/mol in the potential range of −55 to −1220 mV (Figure 2b). The weak sensitivity of E_{app} to the applied potential indicates that the applied potential exerts a similar effect on the energies of the reactants and the activated complex. It can be inferred that the applied potential likely impacts the ethylene hydrogenation activity primarily by altering the surface coverage of adsorbates.

Isotopic Labeling Investigations. Hydrogenation of ethylene with D_2 was conducted at various applied potentials to gain mechanistic insights. A stoichiometric reaction between C_2H_4 and D_2 leads to $C_2H_4D_2$. Other isotopologues of ethane, i.e., $C_2H_xD_{6-x}$ (x = 0−6), could be produced if dissociative adsorption of C_2H_4 occurs on Pt to produce adsorbed C_2H_x (x = 0−3) and H_{ad}. At all potentials investigated (Figure S14c), the mass spectrometry (MS) signal with the highest m/z ratio for ethane is 32 amu, which corresponds to the parent ion of the product in the stoichiometric addition of D_2 to C_2H_4, i.e., $C_2H_4D_2$. Importantly, when ethylene and D_2 were used as the feed, the detected MS signals of 28, 29, 30, 31, and 32 amu deviated substantially from the mass fragmentation pattern of $C_2H_4D_2$,[66−68] suggesting that a mixture of $C_2H_4D_2$, C_2H_5D, and C_2H_6 was produced. There are two possible sources of H_{ad} in the reaction between C_2H_4 and D_2: (1) residual water (H_2O) in acetonitrile and (2) C_2H_4. The former is unlikely to be a substantial H source, as the amount of residual water is far from being able to account for the amount of H incorporated in ethane. For example, ∼12% of ethane produced at −620 mV (close to E_{ocp}) is C_2H_5D (Figure 3a). Assuming one H atom in C_2H_5D comes from the electrochemical reduction of residual H_2O, this would translate to a current density of 0.196 mA/cm^2, which is a factor of ∼100 higher than the experimentally observed current density. Control experiment in which 50 μL of water was intentionally introduced to the acetonitrile electrolyte produced a comparable amount of ethane to the experiment without added water (Figure S15), confirming that the trace amount of residual water in acetonitrile did not contribute to the observed activity in any significant manner. Thus, the formation of C_2H_5D and C_2H_6 is a clear indication that H_{ad} formed in the dissociative adsorption of ethylene serves as a H source in the ethylene hydrogenation (Figure S14d). Further, the fractions of these three isotopologues of ethane could be estimated by deconvoluting the MS spectra (Figure S14e) with the reported mass fragmentation patterns of these compounds (Figure 3a, Table S2, and Supporting Note II). As the applied potential on Pt/C increases from −920 to −55 mV, the fractions of ethane isotopologues with fewer D atoms, i.e., C_2H_5D and C_2H_6, increase at the expense of $C_2H_4D_2$ (Figure 3a). This trend indicates that the H_{ad}/D_{ad} ratio on the surface increases with the increase in the applied potential, suggesting that positive potentials favor the dissociative adsorption of ethylene on Pt and in turn higher coverages of the molecularly adsorbed ethylene precursor. This is consistent with the declining trend in the ethylene reaction order as the applied potential increases (Figure 2a). Dissociative adsorption of ethylene is well documented in the surface science literature to form the inactive ethylidyne (C_2H_3) on Pt and a H_{ad}.[63−65] It could be inferred that more positive applied potentials favor the dissociative adsorption of ethylene on Pt, which could also explain the gradual catalyst deactivation with reaction time caused by the formation of inactive and site-blocking species like ethylidyne (Figure S16). The positive correlation between the H_{ad}/D_{ad} ratio and the applied potential is also evidence against residual water in acetonitrile being the H source because more negative potentials should favor the electrochemical reduction of protons in H_2O to H_{ad} and lead to higher fractions of ethane isotopologues with more H atoms. The opposite was observed.

Isotopic compositions of ethylene, hydrogen, and ethane also provide insights into the reaction network. The ratio between the MS signals of 29 and 28 amu of ethylene does not change with the applied potential after the reaction between C_2H_4 and D_2 (Figure S17a), and is identical within experimental errors to that of C_2H_4 in the feed. This indicates (1) dissociative adsorption of ethylene is essentially irreversible under the conditions investigated in this work, i.e., the rehydrogenation of C_2H_3 by D_{ad} to form C_2H_3D does not occur at any detectable level and (2) the hydrogenation of C_2H_4 with D_{ad} to $C_2H_4D_{ad}$ is also irreversible, otherwise C_2H_3D would be produced via the reverse reaction with $C_2H_4D_{ad}$. Similarly, the ratios among the MS signals of 2, 3, and 4 amu do not depend on the applied potential and are the same as those of D_2 in the feed (Figure

https://doi.org/10.1021/acscatal.3c04258
ACS Catal. 2023, 13, 14570−14579

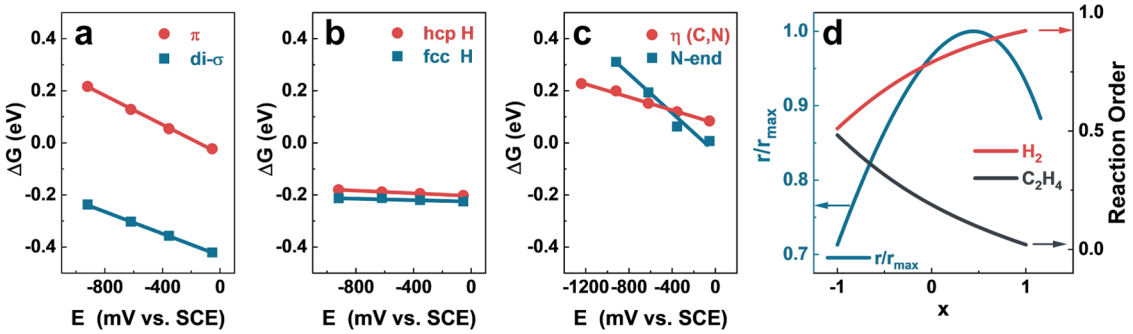

Figure 4. Adsorption Gibbs free energy of (a) ethylene, (b) hydrogen, and (c) acetonitrile with different configurations on Pt(111) at different potentials. (d) Numerical simulations for ethylene hydrogenation rate, reaction orders of ethylene and H_2 vs x ($x = \lambda_{C_2H_4}\Omega$) when $a = 0.012$ and $b = 0.12$. Variables a, b, and x are defined in Supporting Note I.

S17b), suggesting that the recombination of H_{ad} and D_{ad} to form H_2 and D_2 is also negligible. This is likely due to the fast consumption of H_{ad} and D_{ad} in ethylene hydrogenation, making their recombination unlikely. When a mixture of ethane and D_2 (5/95%) was used as the feed under conditions similar to those for ethylene hydrogenation, no detectable level of H−D scrambling was observed in either ethane or D_2 (Figure S18). This is evidence for the irreversibility of ethane desorption in the ethylene hydrogenation. Based on these experimental results, we propose a modified Horiuti−Polanyi mechanism for ethylene hydrogenation on Pt under the conditions employed in this work

Step 1	$C_2H_4+*\rightleftarrows C_2H_4*$	K_1
Step 2	$H_2+2*\rightarrow 2H*$	k_2
Step 3	$CH_3CN+*\rightleftarrows CH_3CN*$	K_3
Step 4	$C_2H_4*+H*\rightarrow C_2H_5*+*$	k_4
Step 5	$C_2H_5*+H*\rightarrow C_2H_6+2*$	k_5

in which dissociative adsorption of H_2, initial hydrogenation of ethylene, and ethane desorption (steps 2, 4, and 5, respectively) are considered irreversible based on the isotopic labeling results described above. The adsorption equilibrium of acetonitrile is included in the reaction network, because the presence of acetonitrile has a pronounced impact on the hydrogenation rate and the reaction orders of ethylene and hydrogen (Figure S13). Adsorption of acetonitrile likely reduces the available surface sites for ethylene and hydrogen to occupy. This reaction mechanism will be employed as the basis of the kinetic analysis in a following section.

Rates of H−D exchange were also determined on Pt/C, Pd/C, and Rh/C at different applied potentials. An equimolar mixture of H_2 and D_2 was employed as the feed to flow into the H cell at the ambient pressure, with the effluent monitored by an online MS. The production rate of HD increases with the rise of the applied potential until −355 mV on Pt/C and Pd/C, before declining precipitously with further increase in the potential (Figures 3b and S19a). The maximum H/D exchange rate is ∼1100 mV on Rh/C (Figure S19b). Importantly, the trends in the H−D exchange are similar to those in the ethylene hydrogenation on all three catalysts investigated. Since both the formation of HD and hydrogenation of ethylene involve adding H_{ad} to another surface-bound intermediate, the shared dependence of both reactions on the potential is unlikely to be coincidental. The steep drop in the HD exchange rate with an increasing potential above −355 mV on Pt/C suggests that the dissociative adsorption of H_2 is suppressed at positive potentials (Figure 3b). This is consistent with the observation that H_{ad} produced in the dissociative adsorption of ethylene becomes a more substantial source of H, as compared to D_{ad} from D_2, in ethylene hydrogenation with D_2 at −55 mV (Figure 3a). The potential cause for the increase in the H−D exchange rate with potential at more negative potentials will be discussed in the following sections.

Impact of Applied Potential on Adsorption Energy. Adsorption Gibbs free energies (ΔG) of hydrogen, ethylene, and acetonitrile on Pt were computed with density functional theory (DFT)-based calculations at different potentials (Figure 4a−c, computational details included in the Methods section in the Supporting Information). Two adsorption configurations were considered for each adsorbate on Pt(111), i.e., ethylene adsorbed via π and di-σ configurations,[54] H adsorbed on the FCC and HCP sites,[55] and acetonitrile adsorbed on the N end and in the η(C, N) configuration[69] (Figure S20). ΔG of all three adsorbates becomes more negative (stronger adsorption) as the potential becomes more positive (Figure 4a−c). Since ΔG values of two adsorption configurations for hydrogen and ethylene differ significantly, only the configurations with more negative ΔG values (stronger adsorption) are considered further, i.e., ethylene adsorbed in the di-σ configuration and H adsorbed on FCC sites. At any given potential, ΔG exhibits the following sequence: ethylene < hydrogen < acetonitrile. The calculated ΔG of acetonitrile is 0.3−0.5 eV more positive than those for ethylene and hydrogen within the potential range investigated. However, acetonitrile exhibits a pronounced impact on ethylene hydrogenation, either in vapor or as the liquid solvent. Likely, this inconsistence is caused by the high concentration (activity) of acetonitrile as the solvent at the interface. It could be deduced that the surface coverage of ethylene is significantly lower in the presence than in the absence of acetonitrile. The potential-dependent bands in the surface-enhanced infrared absorption (SEIRA) spectra of acetonitrile also support the specific adsorption of acetonitrile on the electrode surface (Figure S21), which is consistent with the literature.[50,51,70,71] It can be inferred that, given that the coverage of more strongly adsorbed ethylene is reduced due to the site competition with acetonitrile, the reduction in the H coverage is expected to be even more pronounced due to the presence of acetonitrile.

Relative sensitivities of ΔG among adsorbates could have a decisive effect on the observed hydrogenation reactivity. The sensitivity of ΔG toward potential is much weaker for hydrogen than ethylene and acetonitrile (Figure 4a−c), which is consistent with previous reports.[72,73] As the applied potential becomes more positive from ∼ −1000 mV, the adsorption of

https://doi.org/10.1021/acscatal.3c04258
ACS Catal. 2023, 13, 14570−14579

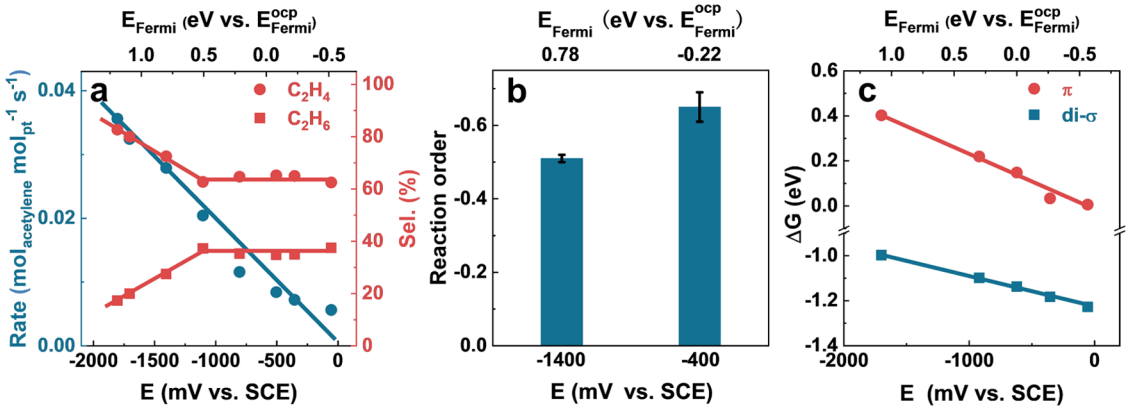

Figure 5. (a) Rate and selectivity of acetylene hydrogenation at different applied potentials on Pt/C. (b) Reaction order of acetylene in its hydrogenation on Pt/C at different applied potentials. (c) Adsorption Gibbs free energy of acetylene with different adsorbed configurations on Pt(111) at different potentials.

ethylene and acetonitrile grows much faster with increasing potentials than that of H_{ad}, leading to lower coverages of H_{ad}. The destabilization of H_{ad} is expected to make it more active toward hydrogenating other surface intermediates, e.g., D_{ad} and ethylene in the formation of HD and ethane, respectively. The combined effect of H_{ad} coverage and activity leads to the volcano-shaped dependence of the hydrogenation chemistry on the applied potential, consistent with the Sabatier principle. At potentials below −355 mV, the beneficial effect of the higher activity of H_{ad} is the dominant factor, so that both HD exchange and ethylene hydrogenation rates increase with potential. The diminished H_{ad} coverage outweighs the activity of H_{ad} at potentials above −355 mV, leading to a precipitous drop in the rates of both HD exchange and ethylene hydrogenation.

Kinetic Modeling. A kinetic model built based on the proposed reaction steps (Steps 1−5) is able to capture key experimental observations. The impact of the applied potential on the adsorbates is modeled via the effective field approach proposed by Vayenas et al.; i.e., only the interaction of dipole moment of the surface adsorbates with the interfacial electric field is considered. Electrochemical potentials for adsorbed ethylene ($\bar{\mu}_{C_2H_4*}$) and acetonitrile ($\bar{\mu}_{CH_3CN*}$) can be expressed as

$$\bar{\mu}_{C_2H_4*} = \mu^0_{C_2H_4*} + RT\ln\frac{\theta_{C_2H_4*}}{\theta_*} - \mathrm{RT}\cdot\lambda_{C_2H_4}\Omega \quad (1)$$

$$\bar{\mu}_{CH_3CN*} = \mu^0_{CH_3CN*} + RT\ln\frac{\theta_{CH_3CN*}}{\theta_*} - RT\cdot\lambda_{CH_3CN}\Omega \quad (2)$$

where $\mu^0_{C_2H_4*}$ and $\mu^0_{CH_3CN*}$ are the standard chemical potentials of adsorbed ethylene and acetonitrile, respectively, at the reference state with a surface coverage of 0.5. $\theta_{C_2H_4*}$, θ_{CH_3CN*}, and θ_* are the fractional coverage for ethylene, acetonitrile, and the unoccupied site, respectively. $\lambda_{C_2H_4}$ and λ_{CH_3CN} are the partial electron-transfer parameters of adsorbed ethylene and acetonitrile, respectively. λ is positive for ethylene and acetonitrile, meaning that they donate electrons to the surface.[35,37] The dimensionless variable Ω represents the potential drop across the double layer, with negative values associated with negatively charged surface and vice versa.[74,75] Electrochemical potentials of adsorbed ethylene and acetonitrile decrease (more stable) with rising applied potentials. This is consistent with the computed results that the adsorption of ethylene and acetonitrile becomes stronger with increasing potential (Figure 4a−c). Based on the proposed modified Horiuti−Polanyi mechanism, the rate expression for the ethylene hydrogenation rate could be derived by applying pseudo steady-state approximation for C_2H_5* and H* (derivation included in Supporting Note I)

$$r = \frac{k_2 P_{H_2}}{\left[\left(K_1 + \frac{K_1 k_4}{k_5}\right)P_{C_2H_4}\exp(\lambda_{C_2H_4}\Omega) + \frac{k_2 P_{H_2}}{k_4 K_1 P_{C_2H_4}}\exp(-\lambda_{C_2H_4}\Omega) + K_3 a_{CH_3CN}\exp(\lambda_{CH_3CN}\Omega) + 1\right]^2} \quad (3)$$

in which K_1, k_2, K_3, k_4, and k_5 are the equilibrium/rate constants of Steps 1−5. $P_{C_2H_4}$ and P_{H_2} are the partial pressures of ethylene and hydrogen, respectively. The potential dependence of the rate is manifested in the presence of Ω in the denominator in eq 3. Reaction orders of hydrogen (n_{H_2}) and ethylene ($n_{C_2H_4}$) can be obtained by taking the partial derivative of ln r with respect to ln P_{H_2} and ln $P_{C_2H_4}$, respectively

$$n_{C_2H_4} = 2(\theta_H - \theta_{C_2H_4} - \theta_{C_2H_5}) \quad (4)$$

$$n_{H_2} = 1 - 2\theta_H \quad (5)$$

Adding eqs 4 and 5 leads to

$$n_{C_2H_4} + n_{H_2} = 1 - 2(\theta_{C_2H_4} + \theta_{C_2H_5}) \quad (6)$$

Sum of measured reaction orders of ethylene and hydrogen is close to unity (Figure 2a), so eq 6 suggests that the combined coverage of molecularly adsorbed ethylene and C_2H_5* is close to zero. This is consistent with the positive reaction order of ethylene. It can be further estimated from the measured reaction order of ethylene and the low value of $\theta_{C_2H_4} + \theta_{C_2H_5}$ that θ_H is at or below ∼0.2. The measured reaction orders of hydrogen are always higher than those of ethylene, suggesting that the coverage of ethylene should be higher than that of H*. This discrepancy indicates that the absolute coverage values of surface intermediates are semiquantitative at best based on this simple kinetic model. However, it is important to note that it correctly predicts that $\theta_{C_2H_4}$, $\theta_{C_2H_5}$, and θ_H combined does not occupy a significant fraction of surface sites. This agrees with the severe inhibiting effect of acetonitrile, whose adsorption likely

https://doi.org/10.1021/acscatal.3c04258
ACS Catal. 2023, 13, 14570−14579

prevents a substantial fraction of surface sites from taking part in the ethylene hydrogenation reaction.

Numerical simulations were conducted to gain insights into the dependence of $n_{C_2H_4}$, n_{H_2}, and r on x ($x = \lambda_{C_2H_4}\Omega$). A volcano-shaped dependence of r on x can be obtained on a wide range of reasonable values of K_1, k_2, K_3, k_4, and k_5 (Figures 4d and S22, Supporting Note I), confirming that the proposed kinetic model is able to capture key features of the reaction system. The first and second terms in the denominator of eq 3 correspond to the coverage of C_2H_4*/C_2H_5* and H*, respectively. The fact that they have opposite dependence on x, or the applied potential, gives rise to the volcano-shaped trend. This is caused by the contrasting trends of the adsorption free energy vs the applied potential for hydrogen and ethylene relative to that of acetonitrile; i.e., the difference in the adsorption free energies between ethylene and acetonitrile becomes greater as the potential increases, while the difference in the adsorption free energies between hydrogen and acetonitrile becomes smaller (Figure 4a−c). In addition, $n_{C_2H_4}$ is predicted to increase with potential and is the opposite for n_{H_2}. When the rate (r) is ploted against the applied potential (x) with parameters confined by the range of experimentally determined ethylene and H_2 reaction orders, a volcano-shaped dependence of r on x is always obtained (Supporting Note I). These predictions are consistent with the measured results (Figures 1c and 2a), further supporting the reliability of the proposed mechanism.

Impact of Applied Potential on Acetylene Hemihydrogenation. To establish the generality of the electric polarization and shifts in the Fermi level on heterogeneous catalysis reactions, we conducted acetylene hydrogenation on Pt/C in a similar configuration. In contrast to the ethylene hydrogenation rate, the acetylene hydrogenation rate increases monotonically with the decrease of the applied potential from −55 to −1800 mV (Figure 5a). Importantly, the product distribution in acetylene hydrogenation is also potential dependent (Figure 5a). When the potential is more positive than −1100 mV, the selectivity of ethylene is maintained at ∼60%. Meanwhile, the ethylene selectivity increases almost linearly with the decrease of the applied potential when the applied potential is more negative than −1100 mV. A ∼90% selectivity for ethylene is achieved at −1800 mV. Reductive currents in all acetylene hydrogenation experiments were at least 1 order of magnitude smaller than those required to reach measured rates of ethylene and ethane production (Figure S23). Thus, electrocatalytic hydrogenation of acetylene is negligible compared to the thermocatalytic pathway. The ethylene production rate is enhanced by a factor of ∼10 when decreasing the applied potential from −55 to −1800 mV, demonstrating the substantial impact of the applied potential on the catalytic activity.

Applied potential has a significant impact on the reaction order of acetylene. Reaction orders of acetylene were determined to be −0.65 and −0.51 at −400 and −1400 mV on Pt/C, respectively (Figure 5b). The negative reaction order of acetylene indicates that the high coverage of acetylene limits the density of sites available for the dissociative adsorption of H_2 to form H_{ad}, which suppresses the reaction rate. This is consistent with the calculated ΔG values of acetylene in the di-σ configuration on Pt of < −1.0 eV within the potential range of −55 to −1700 mV (Figure 5c).[76] Calculated ΔG suggests that acetylene adsorbs more strongly at more positive potentials, which is consistent with the more negative reaction order at −400 mV compared with that at −1400 mV. The monotonic increase in the acetylene conversion rate with the decrease of the potential is in contrast with the volcano-shaped trends for HD exchange and ethylene hydrogenation (Figures 1c and 3b). This could be attributed to the strong adsorption of acetylene on the Pt surface, which makes the availability of surface sites for the dissociative adsorption of hydrogen, i.e., the low H_{ad} coverage, the primary limiting factor for the reaction.

The trend of acetylene hydrogenation selectivity could be rationalized by the relative adsorption strengths of ethylene and acetylene on Pt at different applied potentials. According to calculated ΔG and measured reaction orders, acetylene adsorbs on Pt significantly more strongly than ethylene and hydrogen, so that the rate of acetylene conversion is largely determined by the coverage of H_{ad}. The weakening adsorption energy of acetylene with decreasing potential and the relatively insensitivity of the hydrogen-binding energy toward potential are expected to increase the H_{ad} coverage at more negative potentials, which in turn enhances the acetylene conversion rate. Selectivities for ethylene and ethane are likely impacted by two countervailing effects of the applied potential: (1) H_{ad} coverage and (2) surface lifetime of ethylene formed in acetylene hydrogenation. Calculated ΔG and measured reaction orders suggest that H_{ad} coverage rises with decreasing potential, while the ΔG of ethylene becomes less negative at more negative potentials, indicating lower coverage and shorter surface lifetime of the formed ethylene. As the applied potential decreases from −55 to −1105 mV, the promotional effect of a higher H_{ad} coverage is offset by the shorter surface lifetime of ethylene in its hydrogenation, leading to a constant ethylene to ethane ratio. As the applied potential is decreased below −1105 mV, the ethylene hydrogenation rate is mainly limited by the surface lifetime (coverage) of ethylene, while the increased H_{ad} coverage primarily benefits the hydrogenation of acetylene, which remains the most abundant surface adsorbates. These results highlight the possibility of leveraging electric polarization to tune the product distribution in thermocatalytic reactions by altering the surface adsorption energy and coverage of adsorbates.

CONCLUSIONS

In summary, we demonstrate that externally applied potential could impact the rate and selectivity of thermocatalytic hydrogenation of ethylene and acetylene on Pt, Pd, and Rh surfaces. The effect of the electric polarization and associated shift in the Fermi level of the metal catalyst on the reaction kinetics could be largely rationalized by the altered coverage of the key surface intermediates. A modified Horiuti−Polanyi mechanism was proposed for the Pt-catalyzed ethylene hydrogenation reaction. By adopting the effective potential method to account for the impact of the electric polarization, the proposed kinetic model is able to qualitatively reproduce the key features of the impact of the potential on the reaction, i.e., the volcano-shaped dependence of the rate on the applied potential and the trend of reaction orders of both ethylene and acetylene. The generality of the impact of the Fermi level shift induced by the applied potential on thermocatalytic reactions was further supported by the activity and selectivity tuning in the hydrogenation of acetylene on Pt/C, where both the rate of acetylene conversion and the selectivity for ethylene could be substantially enhanced when the surface was negatively biased. Results reported in this work highlight the promise of leveraging the electric polarization to understand the impact of the Fermi

https://doi.org/10.1021/acscatal.3c04258
ACS Catal. 2023, 13, 14570−14579

level on the catalytic mechanisms and serve as a unique dimension to optimize performance.

■ ASSOCIATED CONTENT

Supporting Information

The Supporting Information is available free of charge at https://pubs.acs.org/doi/10.1021/acscatal.3c04258.

Materials; methods; characterizations; computational details; supporting notes; supporting tables; and supporting figures (PDF)

■ AUTHOR INFORMATION

Corresponding Authors

Hai Xiao − *Department of Chemistry and Key Laboratory of Organic Optoelectronics & Molecular Engineering of Ministry of Education, Tsinghua University, Beijing 100084, China;* orcid.org/0000-0001-9399-1584; Email: haixiao@tsinghua.edu.cn

Bingjun Xu − *Beijing National Laboratory for Molecular Sciences, College of Chemistry and Molecular Engineering, Peking University, Beijing 100871, China;* orcid.org/0000-0002-2303-257X; Email: b_xu@pku.edu.cn.

Authors

Qikai Shen − *Beijing National Laboratory for Molecular Sciences, College of Chemistry and Molecular Engineering, Peking University, Beijing 100871, China*

Hanwen Yang − *Beijing National Laboratory for Molecular Sciences, College of Chemistry and Molecular Engineering, Peking University, Beijing 100871, China*

Kaiyue Zhao − *Beijing National Laboratory for Molecular Sciences, College of Chemistry and Molecular Engineering, Peking University, Beijing 100871, China;* orcid.org/0000-0003-3923-7788

Leyu Liu − *Department of Chemistry and Key Laboratory of Organic Optoelectronics & Molecular Engineering of Ministry of Education, Tsinghua University, Beijing 100084, China*

Qiwen Sun − *Beijing National Laboratory for Molecular Sciences, College of Chemistry and Molecular Engineering, Peking University, Beijing 100871, China*

Xiaoxia Chang − *Beijing National Laboratory for Molecular Sciences, College of Chemistry and Molecular Engineering, Peking University, Beijing 100871, China*

Complete contact information is available at: https://pubs.acs.org/10.1021/acscatal.3c04258

Author Contributions

§Q.S. and H.Y. contributed equally. The manuscript was written through contributions of all authors. All authors have given approval to the final version of the manuscript. These authors contributed equally.

Notes

The authors declare no competing financial interest.

■ ACKNOWLEDGMENTS

This work is supported by the National Key R&D Program of China (No. 2021YFA1501003). Q.S. acknowledges support from the Chinese Postdoctoral Science Foundation (No. 2022M710205).

■ REFERENCES

(1) Taylor, H. S. A theory of the catalytic surface. *Proc. R. Soc. London, Ser. A* **1925**, *108* (745), 105−111.

(2) Coq, B.; Figueras, F. Structure−activity relationships in catalysis by metals: some aspects of particle size, bimetallic and supports effects. *Coord. Chem. Rev.* **1998**, *178*−*180*, 1753−1783.

(3) Montgomery, S. L.; Pushpanath, A.; Heath, R. S.; Marshall, J. R.; Klemstein, U.; Galman, J. L.; Woodlock, D.; Bisagni, S.; Taylor, C. J.; Mangas-Sanchez, J.; Ramsden, J. I.; Dominguez, B.; Turner, N. J. Characterization of imine reductases in reductive amination for the exploration of structure-activity relationships. *Sci. Adv.* **2020**, *6* (21), No. eaay9320.

(4) Sun, Y.; Liao, H.; Wang, J.; Chen, B.; Sun, S.; Ong, S. J. H.; Xi, S.; Diao, C.; Du, Y.; Wang, J.-O.; Breese, M. B. H.; Li, S.; Zhang, H.; Xu, Z. J. Covalency competition dominates the water oxidation structure−activity relationship on spinel oxides. *Nat. Catal.* **2020**, *3* (7), 554−563.

(5) Vogt, C.; Weckhuysen, B. M. The concept of active site in heterogeneous catalysis. *Nat. Rev. Chem.* **2022**, *6* (2), 89−111.

(6) Luo, Z.; Zhao, G.; Pan, H.; Sun, W. Strong metal−support interaction in heterogeneous catalysts. *Adv. Energy Mater.* **2022**, *12* (37), No. 2201395.

(7) Pacchioni, G.; Freund, H. J. Controlling the charge state of supported nanoparticles in catalysis: lessons from model systems. *Chem. Soc. Rev.* **2018**, *47* (22), 8474−8502.

(8) Campbell, C. T. Catalyst-support interactions: Electronic perturbations. *Nat. Chem.* **2012**, *4* (8), 597−598.

(9) Ahmadi, M.; Mistry, H.; Roldan Cuenya, B. Tailoring the catalytic properties of metal nanoparticles via support interactions. *J. Phys. Chem. Lett.* **2016**, *7* (17), 3519−3533.

(10) van Deelen, T. W.; Hernández Mejía, C.; de Jong, K. P. Control of metal-support interactions in heterogeneous catalysts to enhance activity and selectivity. *Nat. Catal.* **2019**, *2* (11), 955−970.

(11) Rajaram, J.; Narula, A. P.; Chawla, H. P.; Dev, S. Semi-hydrogenation of acetylenes - modified lindlar catalyst. *Tetrahedron* **1983**, *39* (13), 2315−2322, DOI: 10.1016/S0040-4020(01)91960-X.

(12) Chen, G.; Xu, C.; Huang, X.; Ye, J.; Gu, L.; Li, G.; Tang, Z.; Wu, B.; Yang, H.; Zhao, Z.; Zhou, Z.; Fu, G.; Zheng, N. Interfacial electronic effects control the reaction selectivity of platinum catalysts. *Nat. Mater.* **2016**, *15* (5), 564−569.

(13) Wang, L.; Guan, E.; Zhang, J.; Yang, J.; Zhu, Y.; Han, Y.; Yang, M.; Cen, C.; Fu, G.; Gates, B. C.; Xiao, F.-S. Single-site catalyst promoters accelerate metal-catalyzed nitroarene hydrogenation. *Nat. Commun.* **2018**, *9* (1), No. 1362.

(14) Pan, Y.; Zhang, C.; Liu, Z.; Chen, C.; Li, Y. Structural regulation with atomic-level precision: From single-atomic site to diatomic and atomic interface catalysis. *Matter* **2020**, *2* (1), 78−110.

(15) Hu, Z.; Li, B.; Sun, X.; Metiu, H. Chemistry of doped oxides: The activation of surface oxygen and the chemical compensation effect. *J. Phys. Chem. C* **2011**, *115* (7), 3065−3074.

(16) Mammen, N.; Narasimhan, S.; de Gironcoli, S. Tuning the morphology of gold clusters by substrate doping. *J. Am. Chem. Soc.* **2011**, *133* (9), 2801−2803.

(17) Lykhach, Y.; Kozlov, S. M.; Skala, T.; Tovt, A.; Stetsovych, V.; Tsud, N.; Dvorak, F.; Johanek, V.; Neitzel, A.; Myslivecek, J.; Fabris, S.; Matolin, V.; Neyman, K. M.; Libuda, J. Counting electrons on supported nanoparticles. *Nat. Mater.* **2016**, *15* (3), 284−288.

(18) Yan, H.; Yang, C.; Shao, W. P.; Cai, L. H.; Wang, W. W.; Jin, Z.; Jia, C. J. Construction of stabilized bulk-nano interfaces for highly promoted inverse CeO_2/Cu catalyst. *Nat. Commun.* **2019**, *10* (1), No. 3470.

(19) Green, I. X.; Tang, W.; Neurock, M.; Yates, J. T., Jr. Spectroscopic observation of dual catalytic sites during oxidation of CO on a Au/TiO_2 catalyst. *Science* **2011**, *333* (6043), 736−739.

(20) Macino, M.; Barnes, A. J.; Althahban, S. M.; Qu, R.; Gibson, E. K.; Morgan, D. J.; Freakley, S. J.; Dimitratos, N.; Kiely, C. J.; Gao, X.; Beale, A. M.; Bethell, D.; He, Q.; Sankar, M.; Hutchings, G. J. Tuning of catalytic sites in Pt/TiO_2 catalysts for the chemoselective hydrogenation of 3-nitrostyrene. *Nat. Catal.* **2019**, *2* (10), 873−881.

(21) Li, Z.; Cui, Y.; Wu, Z.; Milligan, C.; Zhou, L.; Mitchell, G.; Xu, B.; Shi, E.; Miller, J. T.; Ribeiro, F. H.; Wu, Y. Reactive metal−support interactions at moderate temperature in two-dimensional niobium-carbide-supported platinum catalysts. *Nat. Catal.* **2018**, *1* (5), 349−355.
(22) Herrmann, J. M. Electronic effects in strong metal-support intaractions on titania deposited metal catalysts. *J. Catal.* **1984**, *89* (2), 404−412.
(23) Nilsson, A.; Pettersson, L. G. M.; Hammer, B.; Bligaard, T.; Christensen, C. H.; Nørskov, J. K. The electronic structure effect in heterogeneous catalysis. *Catal. Lett.* **2005**, *100* (3−4), 111−114.
(24) Zhu, W.; Zhang, L.; Liu, S.; Li, A.; Yuan, X.; Hu, C.; Zhang, G.; Deng, W.; Zang, K.; Luo, J.; Zhu, Y.; Gu, M.; Zhao, Z. J.; Gong, J. Enhanced CO_2 electroreduction on neighboring Zn/Co monomers by electronic effect. *Angew. Chem., Int. Ed.* **2020**, *59* (31), 12664−12668.
(25) Shi, Y.; Ma, Z. R.; Xiao, Y. Y.; Yin, Y. C.; Huang, W. M.; Huang, Z. C.; Zheng, Y. Z.; Mu, F. Y.; Huang, R.; Shi, G. Y.; Sun, Y. Y.; Xia, X. H.; Chen, W. Electronic metal-support interaction modulates single-atom platinum catalysis for hydrogen evolution reaction. *Nat. Commun.* **2021**, *12* (1), No. 3021.
(26) Luo, Y.; Wang, D. Enhancing heterogeneous catalysis by electronic property regulation of single atom catalysts. *Acta Phys.-Chim. Sin.* **2023**, *39* (9), No. 221202, DOI: 10.3866/PKU.WHXB202212020.
(27) Pancharatnam, S.; Huggins, R. A.; Mason, D. M. Catalytic decomposition of nitric oxide on zirconia by electrolytic removal of oxygen. *J. Electrochem. Soc.* **1975**, *122* (7), 869 DOI: 10.1149/1.2134364.
(28) Stoukides, M.; Vayenas, C. G. The effect of electrochemical oxygen pumping on the rate and selectivity of ethylene oxidation on polycrystalline silver. *J. Catal.* **1981**, *70* (1), 137−146.
(29) Vayenas, C. G.; Bebelis, S.; Neophytides, S. Non-faradaic electrochemical modification of catalytic activity. *J. Phys. Chem. A* **1988**, *92* (18), 5083−5085.
(30) Vayenas, C. G.; Lee, B.; Michaels, J. Kinetics, limit-cycles, and mechanism of the ethylene oxidation on platinum. *J. Catal.* **1980**, *66* (1), 36−48.
(31) Vayenas, C. G.; Bebelis, S.; Ladas, S. Dependence of catalytic rates on catalyst work function. *Nature* **1990**, *343* (6259), 625−627.
(32) Hajar, Y. M.; Treps, L.; Michel, C.; Baranova, E. A.; Steinmann, S. N. Theoretical insight into the origin of the electrochemical promotion of ethylene oxidation on ruthenium oxide. *Catal. Sci. Technol.* **2019**, *9* (21), 5915−5926.
(33) Panaritis, C.; Hajar, Y. M.; Treps, L.; Michel, C.; Baranova, E. A.; Steinmann, S. N. Demystifying the Atomistic Origin of the Electric Field Effect on Methane Oxidation. *J. Phys. Chem. Lett.* **2020**, *11* (17), 6976−6981.
(34) Vayenas, C. G.; Brosda, S.; Pliangos, C. Rules and mathematical modeling of electrochemical and chemical promotion. *J. Catal.* **2001**, *203* (2), 329−350.
(35) Brosda, S.; Vayenas, C. G. Rules and mathematical modeling of electrochemical and classical promotion. *J. Catal.* **2002**, *208* (1), 38−53.
(36) Lambert, R. M.; Williams, F.; Palermo, A.; Tikhov, M. S. Modelling alkali promotion in heterogeneous catalysis: in situ electrochemical control of catalytic reactions. *Top. Catal.* **2000**, *13* (1−2), 91−98.
(37) Vayenas, C. G.; Brosda, S. Electron donation−backdonation and the rules of catalytic promotion. *Top. Catal.* **2014**, *57* (14−16), 1287−1301.
(38) Neophytides, S. G.; Tsiplakides, D.; Stonehart, P.; Jaksic, M. M.; Vayenas, C. G. Electrochemical enhancement of a catalytic reaction in aqueous solution. *Nature* **1994**, *370* (6484), 45−47.
(39) Sapountzi, F. M.; Tsampas, M. N.; Vayenas, C. G. Electrochemical promotion of CO conversion to CO_2 in PEM fuel cell PROX reactor. *Catal. Today* **2009**, *146* (3−4), 319−325.
(40) Sanabria-Chinchilla, J.; Asazawa, K.; Sakamoto, T.; Yamada, K.; Tanaka, H.; Strasser, P. Noble metal-free hydrazine fuel cell catalysts: EPOC effect in competing chemical and electrochemical reaction pathways. *J. Am. Chem. Soc.* **2011**, *133* (14), 5425−5431.
(41) Lim, C. W.; Hülsey, M. J.; Yan, N. Non-faradaic promotion of ethylene hydrogenation under oscillating potentials. *JACS Au* **2021**, *1* (5), 536−542.
(42) Cai, F.; Gao, D.; Zhou, H.; Wang, G.; He, T.; Gong, H.; Miao, S.; Yang, F.; Wang, J.; Bao, X. Electrochemical promotion of catalysis over Pd nanoparticles for CO_2 reduction. *Chem. Sci.* **2017**, *8* (4), 2569−2573.
(43) Qi, X.; Shinagawa, T.; Lu, X.; Yui, Y.; Ibe, M.; Takanabe, K. Surface coverage control for dramatic enhancement of thermal CO oxidation by precise potential tuning of metal supported catalysts. *Chem. Sci.* **2022**, *13* (33), 9774−9783.
(44) Ryu, J.; Surendranath, Y. Polarization-induced local pH swing promotes Pd-catalyzed CO_2 hydrogenation. *J. Am. Chem. Soc.* **2020**, *142* (31), 13384−13390.
(45) Che, F.; Gray, J. T.; Ha, S.; McEwen, J.-S. Catalytic water dehydrogenation and formation on nickel: Dual path mechanism in high electric fields. *J. Catal.* **2015**, *332*, 187−200.
(46) Singh, N.; Lee, M.-S.; Akhade, S. A.; Cheng, G.; Camaioni, D. M.; Gutiérrez, O. Y.; Glezakou, V.-A.; Rousseau, R.; Lercher, J. A.; Campbell, C. T. Impact of pH on Aqueous-Phase Phenol Hydrogenation Catalyzed by Carbon-Supported Pt and Rh. *ACS Catal.* **2019**, *9* (2), 1120−1128.
(47) Wesley, T. S.; Roman-Leshkov, Y.; Surendranath, Y. Spontaneous Electric Fields Play a Key Role in Thermochemical Catalysis at Metal-Liquid Interfaces. *ACS Cent. Sci.* **2021**, *7* (6), 1045−1055.
(48) Wesley, T. S.; Hulsey, M. J.; Westendorff, K. S.; Lewis, N. B.; Crumlin, E. J.; Roman-Leshkov, Y.; Surendranath, Y. Metal nanoparticles supported on a nonconductive oxide undergo pH-dependent spontaneous polarization. *Chem. Sci.* **2023**, *14* (26), 7154−7160.
(49) Singh, N.; Nguyen, M.-T.; Cantu, D. C.; Mehdi, B. L.; Browning, N. D.; Fulton, J. L.; Zheng, J.; Balasubramanian, M.; Gutiérrez, O. Y.; Glezakou, V.-A.; Rousseau, R.; Govind, N.; Camaioni, D. M.; Campbell, C. T.; Lercher, J. A. Carbon-supported Pt during aqueous phenol hydrogenation with and without applied electrical potential: X-ray absorption and theoretical studies of structure and adsorbates. *J. Catal.* **2018**, *368*, 8−19.
(50) Ledezma-Yanez, I.; Díaz-Morales, O.; Figueiredo, M. C.; Koper, M. T. M. Hydrogen oxidation and hydrogen evolution on a platinum electrode in acetonitrile. *ChemElectroChem* **2015**, *2* (10), 1612−1622.
(51) Ledezma-Yanez, I.; Koper, M. T. M. Influence of water on the hydrogen evolution reaction on a gold electrode in acetonitrile solution. *J. Electroanal. Chem.* **2017**, *793*, 18−24.
(52) Dubouis, N.; Serva, A.; Salager, E.; Deschamps, M.; Salanne, M.; Grimaud, A. The fate of water at the electrochemical interfaces: Electrochemical behavior of free water versus coordinating water. *J. Phys. Chem. Lett.* **2018**, *9* (23), 6683−6688.
(53) Shaikhutdinov, S.; Heemeier, M.; Bäumer, M.; Lear, T.; Lennon, D.; Oldman, R. J.; Jackson, S. D.; Freund, H. J. Structure−reactivity relationships on supported metal model catalysts: adsorption and reaction of ethene and hydrogen on $Pd/Al_2O_3/NiAl(110)$. *J. Catal.* **2001**, *200* (2), 330−339.
(54) Watson, G. W.; Wells, R. P. K.; Willock, D. J.; Hutchings, G. J. Density functional theory calculations on the interaction of ethene with the {111} surface of platinum. *J. Phys. Chem. B* **2000**, *104* (27), 6439−6446.
(55) Watson, G. W.; Wells, R. P. K.; Willock, D. J.; Hutchings, G. J. A comparison of the adsorption and diffusion of hydrogen on the {111} surfaces of Ni, Pd, and Pt from density functional theory calculations. *J. Phys. Chem. B* **2001**, *105* (21), 4889−4894.
(56) Adams, J. S.; Kromer, M. L.; Rodriguez-Lopez, J.; Flaherty, D. W. Unifying Concepts in Electro- and Thermocatalysis toward Hydrogen Peroxide Production. *J. Am. Chem. Soc.* **2021**, *143* (21), 7940−7957.
(57) Liu, X.; Conte, M.; Elias, D.; Lu, L.; Morgan, D. J.; Freakley, S. J.; Johnston, P.; Kiely, C. J.; Hutchings, G. J. Investigation of the active species in the carbon-supported gold catalyst for acetylene hydrochlorination. *Catal. Sci. Technol.* **2016**, *6* (13), 5144−5153.
(58) Michaelson, H. B. The work function of the elements and its periodicity. *J. Appl. Phys.* **1977**, *48* (11), 4729−4733.

(59) Cortright, R. D.; Goddard, S. A.; Rekoske, J. E.; Dumesic, J. A. Kinetic study of ethylene hydrogenation. *J. Catal.* **1991**, *127* (1), 342−353.
(60) Zaera, F.; Somorjai, G. A. Hydrogenation of ethylene over platinum (111) single-crystal surfaces. *J. Am. Chem. Soc.* **1984**, *106* (8), 2288−2293.
(61) Griffiths, K.; Lennard, W. N.; Mitchell, I. V.; Norton, P. R.; Pirug, G.; Bonzel, H. P. Saturated ethylene coverage on Pt(111): a comparison of nuclear reaction analysis and X-ray photoemission data. *Surf. Sci.* **1993**, *284* (1), L389−L393.
(62) Cremer, P. S.; Su, X. C.; Shen, Y. R.; Somorjai, G. A. Ethylene hydrogenation on Pt(111) monitored in situ at high pressures using sum frequency generation. *J. Am. Chem. Soc.* **1996**, *118* (12), 2942−2949.
(63) Zaera, F. Mechanisms for ethylene hydrogenation and H-D exchange over Pt(111). *J. Phys. Chem. A* **1990**, *94* (12), 5090−5095.
(64) Cremer, P. S.; Somorjai, G. A. Surface science and catalysis of ethylene hydrogenation. *J. Chem. Soc., Faraday Trans.* **1995**, *91* (20), 3671−3677, DOI: 10.1039/ft9959103671.
(65) Horiuti, I.; Polanyi, M. Exchange reactions of hydrogen on metallic catalysts. *Trans. Faraday Soc.* **1934**, *30*, 1164−1172, DOI: 10.1039/tf9343001164.
(66) Amenomiya, Y.; Pottie, R. F. Mass spectra of some deuterated ethanes. I. The effect of ionizing voltage. *Can. J. Chem.* **1968**, *46* (10), 1735−1739.
(67) Schissler, D. O.; Thompson, S. O.; Turkevich, J. Behaviour of Paraffin Hydrocarbons on Electron Impact - Synthesis and Mass Spectra of Some Deuterated Paraffin Hydrocarbons. *Discuss. Faraday Soc.* **1951**, *10* (0), 46−53, DOI: 10.1039/df9511000046.
(68) Flynn, J. H.; Hulburt, H. M. The reduction of ethylene platinous chloride with deuterium - The mass spectra of deuterated ethanes 1. *J. Am. Chem. Soc.* **1954**, *76* (13), 3396−3400.
(69) Ludwig, T.; Singh, A. R.; Norskov, J. K. Acetonitrile transition metal interfaces from first principles. *J. Phys. Chem. Lett.* **2020**, *11* (22), 9802−9811.
(70) Suárez-Herrera, M. F.; Costa-Figueiredo, M.; Feliu, J. M. Voltammetry of basal plane platinum electrodes in acetonitrile electrolytes: Effect of the presence of water. *Langmuir* **2012**, *28* (11), 5286−5294.
(71) Villegas, I.; Weaver, M. J. Infrared spectroscopy of model electrochemical interfaces in ultrahigh vacuum: Ionic versus interfacial solvation by acetone and acetonitrile on Pt(111). *J. Am. Chem. Soc.* **1996**, *118* (2), 458−466.
(72) Resasco, J.; Chen, L. D.; Clark, E.; Tsai, C.; Hahn, C.; Jaramillo, T. F.; Chan, K.; Bell, A. T. Promoter effects of alkali metal cations on the electrochemical reduction of carbon dioxide. *J. Am. Chem. Soc.* **2017**, *139* (32), 11277−11287.
(73) Zhang, H.; Goddard, W. A.; Lu, Q.; Cheng, M. J. The importance of grand-canonical quantum mechanical methods to describe the effect of electrode potential on the stability of intermediates involved in both electrochemical CO_2 reduction and hydrogen evolution. *Phys. Chem. Chem. Phys.* **2018**, *20* (4), 2549−2557.
(74) Vernoux, P.; Lizarraga, L.; Tsampas, M. N.; Sapountzi, F. M.; De Lucas-Consuegra, A.; Valverde, J. L.; Souentie, S.; Vayenas, C. G.; Tsiplakides, D.; Balomenou, S.; Baranova, E. A. Ionically conducting ceramics as active catalyst supports. *Chem. Rev.* **2013**, *113* (10), 8192−8260.
(75) Vayenas, C. G.; Brosda, S.; Pliangos, C. The double-layer approach to promotion, electrocatalysis, electrochemical promotion, and metal−support interactions. *J. Catal.* **2003**, *216* (1−2), 487−504.
(76) Medlin, J. W.; Allendorf, M. D. Theoretical study of the adsorption of acetylene on the (111) surfaces of Pd, Pt, Ni, and Rh. *J. Phys. Chem. B* **2003**, *107* (1), 217−223.

https://doi.org/10.1021/acscatal.3c04258
ACS Catal. 2023, 13, 14570−14579